Chemical Science

ROYAL SOCIETY OF CHEMISTRY

EDGE ARTICLE

View Article Online
View Journal | View Issue

Cite this: *Chem. Sci.*, 2023, **14**, 9033

All publication charges for this article have been paid for by the Royal Society of Chemistry

Received 5th July 2023
Accepted 2nd August 2023

DOI: 10.1039/d3sc03435f

rsc.li/chemical-science

Boosting the zinc storage of a small-molecule organic cathode by a desalinization strategy†

Wei Wang,‡[a] Ying Tang,‡[a] Jun Liu,[b] Hongbao Li,*[a] Rui Wang,[a] Longhai Zhang,[a] Fei Liang,[a] Wei Bai,*[a] Lin Zhang[c] and Chaofeng Zhang*[a]

Organic materials offer great potential as electrodes for batteries due to their high theoretical capacity, flexible structural design, and easily accessible materials. However, one significant drawback of organic electrode materials is their tendency to dissolve in the electrolyte. Resazurin sodium salt (RSS) has demonstrated remarkable charge/discharge performance characterized by a voltage plateau and high capacity when utilized as a cathode in aqueous zinc-ion batteries (AZIBs). Unfortunately, the solubility of RSS as a sodium salt continues to pose challenges in AZIBs. In this study, we introduce an RSS-containing organic compound, triresazurin-triazine (TRT), with a porous structure prepared by a desalinization method from the RSS and 2,4,6-trichloro-1,3,5-triazine (TCT). This process retained active groups (carbonyl and nitroxide radical) while generating a highly conjugated structure, which not only inhibits the dissolution in the electrolyte, but also improves the electrical conductivity, enabling TRT to have excellent electrochemical properties. When evaluated as a cathode for AZIBs, TRT exhibits a high reversible capacity of 180 mA h g^{-1}, exceptional rate performance (78 mA h g^{-1} under 2 A g^{-1}), and excellent cycling stability with 65 mA h g^{-1} at 500 mA g^{-1} after 1000 cycles.

Introduction

With the rapid development of electric vehicles and grid storage systems, along with the global concerns surrounding environmental pollution and climate change, there is a growing demand for energy storage solutions to align with sustainable and environmentally friendly development.[1–5] Over the past few decades, extensive research has been dedicated to the practical applications of Li-ion batteries (LIBs) due to their high energy and power density.[6–11] However, LIBs suffer from numerous critical issues, such as the finite availability of lithium metal resources and the hazardous and flammable nature of their electrolytes.[12–14] Consequently, there has been growing interest among researchers in safer rechargeable aqueous zinc-ion batteries (AZIBs). Zinc, a metal abundant in the Earth's crust and stable in the air, offers a high theoretical specific capacity of 820 mA h g^{-1} and a low redox potential (−0.76 V *vs.* SHE) when utilized as an anode in aqueous batteries.[15–19] Aqueous electrolytes offer improved safety and environmental friendliness compared to organic electrolytes due to their non-flammability properties and significantly lower cost.[20–24]

In recent years, the design of cathode materials has played a crucial role in determining the electrochemical performance of AZIBs. Initially, the cathode materials for AZIBs were predominantly inorganic compounds, such as manganese (Mn)-based compounds[25–27] and vanadium (V)-based compounds.[28–30] Despite their high capacity, these materials encounter challenges, such as rapid capacity decay and poor cycle performance, primarily due to unstable structure issues.[31,32] Furthermore, inorganic electrode materials are often accompanied by structural changes because of the insertion or extraction of Zn^{2+}, which is also a drawback of using inorganic materials.[33,34] Organic electrode materials are mainly composed of sustainable elements, for example, C, H, and O, and can be derived from readily available biomass resources.[35–38] Moreover, organic electrode materials offer great design flexibility, enabling the customization of physical properties and electrochemical performance.[39–41] In addition, in organic materials for AZIBs, the redox reaction primarily involves the rearrangement of chemical bonds rather than the insertion or extraction of Zn^{2+}, thus mitigating the extensive structural changes commonly observed in inorganic compounds.[42]

[a]*Institutes of Physical Science and Information Technology, Leibniz International Joint Research Center of Materials Sciences of Anhui Province, Anhui Province Key Laboratory of Environment-Friendly Polymer Materials, Key Laboratory of Structure and Functional Regulation of Hybrid Material (Ministry of Education), Anhui University, Hefei 230601, China. E-mail: lihb@ahu.edu.cn; baiwei@ahu.edu.cn; cfz@ahu.edu.cn*

[b]*School of Materials Science and Engineering, Guangdong Provincial Key Laboratory of Advanced Energy Storage Materials, South China University of Technology, Guangzhou 510640, China*

[c]*Institute for Solid State Physics Laboratory of Nano and Quantum Engineering, Leibniz University Hannover, Appelstrasse 2, 30167 Hannover, Germany*

† Electronic supplementary information (ESI) available. See DOI: https://doi.org/10.1039/d3sc03435f

‡ These authors contributed equally to this work.

Small-molecule organic materials usually show the advantages of high activity and high capacity when acting as the cathode of AZIBs. However, the significant challenges faced by most small-molecule organic materials are their tendency to dissolve easily in the electrolyte, poor conductivity, leading to poor cycling performance, sluggish kinetics, and limited stability.[43] Extensive research has been conducted to enhance the cycle performance of organic electrode materials by refining their molecular structure to tackle solubility issues. Various approaches have been explored to improve battery performance, including polymerization and salinization.[44,45] Nonetheless, it is essential to note that polymers with dense structures can reduce the number of electroactive sites and hinder ion transportation, resulting in a reduced capacity, as well as poor cycling stability and rate capability. Thus, designing a suitable molecular structure that overcomes the limitations associated with polymers while effectively addressing solubility and conductivity concerns and preserving the electrochemical activity of the material remains a significant challenge.

Resazurin sodium salt (RSS) serves as a cathode for AZIBs, displaying an exceptional charge/discharge plateau and a high theoretical capacity. However, the capacity retention of RSS is severely compromised due to solubility and low conductivity issues. In this study, we have successfully synthesized a novel small-molecule organic cathode called triresazurin-triazine (TRT) through a simple synthesis method involving RSS and 2,4,6-trichloro-1,3,5-triazine (TCT). The formation of TRT allows us to effectively address solubility concerns while preserving the electrochemical activity of RSS and eliminating non-redox active sites (Na). Furthermore, the highly conjugated structure and insolubility of TRT contribute to improved electrical conductivity, superior specific capacity, extended cycle life, and enhanced rate performance compared to RSS. This research presents a promising strategy for mitigating solubility issues while maintaining the electrochemical activity of small-molecule organic materials, highlighting a right direction in the development of organic electrode materials for AZIBs.

Experimental section

Synthesis of triresazurin-triazine (TRT)

To obtain the sample, a straightforward reaction was conducted by adding resazurin sodium salt (301.2 mg, 1.2 mmol) and 2,4,6-trichloro-1,3,5-triazine (55.2 mg, 0.3 mmol) to 80 ml of *N*,*N*-dimethylformamide. The mixture was then heated at 160 °C for 24 hours under a nitrogen atmosphere. After cooling to room temperature, the crude product was obtained through vacuum filtration and subsequently washed with abundant deionized water (DI water) to eliminate any excess reactants. Finally, the product was dried under a vacuum at 80 °C for 12 hours, forming the desired black solid.

Material characterization

A Fourier transform infrared spectrometer (FT-IR, Vertex80+-Hyperion2000) was used to determine the chemical bonds and functional groups of TRT. The element content of the product was analyzed using an element analyzer (Vario EL-3). Scanning electron microscopy (SEM, Regulus 8230) was employed to obtain SEM images for observing the morphology. The solubility of TRT in the electrolyte was revealed through UV-vis spectra (SPECORD 210). Thermal stability was studied using thermogravimetric analysis (TGA, TG 209 F3 Tarsus) under an air atmosphere. The surface adsorption properties of TRT were analyzed using an ASAP-2460 surface area analyzer. The BET test was conducted at 200 °C for degassing, then N_2 was used as the protective gas, and the test was carried out under liquid nitrogen. Electron paramagnetic resonance (EPR) spectra were provided using an EPR200M. During the preparation of *ex situ* test samples, the batteries were charged or discharged to reach the desired potential. Afterward, the batteries were disassembled, and the samples were thoroughly rinsed with deionized water to remove any remaining electrolyte residues from the surfaces.

Electrochemical measurements

The working electrodes were composed of active materials, carbon black (Ketjen Black), and polyvinylidene fluoride (PVDF) with a weight ratio of 6 : 2.5 : 1.5. The mass loading of the active material was about 1.0 mg cm^{-2}. The coin-type cells (CR2032) were assembled with the as-prepared material as a cathode, zinc foil as an anode, and 2.0 M zinc sulphate ($ZnSO_4$) as an electrolyte. The electrochemical performance of the battery was evaluated on a Chenhua electrochemical station and NEWARE testing system (5 V/10 mA, Shenzhen, China). The voltage range of the AZIB was 0.4–1.4 V.

Results and discussion

TRT was synthesized using a facile synthesis process, as illustrated in Fig. 1a. The structure and purity of the compounds were verified through FTIR spectra and elemental analysis. The FT-IR spectra depicted in Fig. 1b exhibit comparable absorption peaks between TRT and the reactants (RSS and TCT), indicating that the synthesized TRT largely retains the original structures of RSS and TCT. The observed absorption bands at 1605/1570 cm^{-1} can be attributed to the vibrational modes of carbonyl groups (C=O).[46] Furthermore, the peaks detected at 1497/1483 cm^{-1} and 1270/1273 cm^{-1} can be assigned to triazine rings.[47,48] The spectral features located at 1354/1369 cm^{-1} correspond to nitroxide radicals (N–O$^{\bullet}$), while those found at 1109/1114 cm^{-1} are associated with C–O stretching.[49] In comparison with RSS and TCT, the absorption peak of O–Na was not observed in TRT,[50] and no peak corresponding to C–Cl was detected in TRT.

These findings strongly indicate the successful synthesis of TRT using a simple synthesis process, as illustrated in Fig. 1a. Fig. 1c presents the elemental analysis result of TRT, showing that C accounts for 60.02%, N accounts for 10.57%, and H accounts for 2.97%, which are close to their theoretical values (C, 61.42%; N, 11.02%; and H, 2.36%).

UV-vis spectrum analysis was carried out to further confirm the solubility of RSS and TRT in electrolytes. The UV spectra

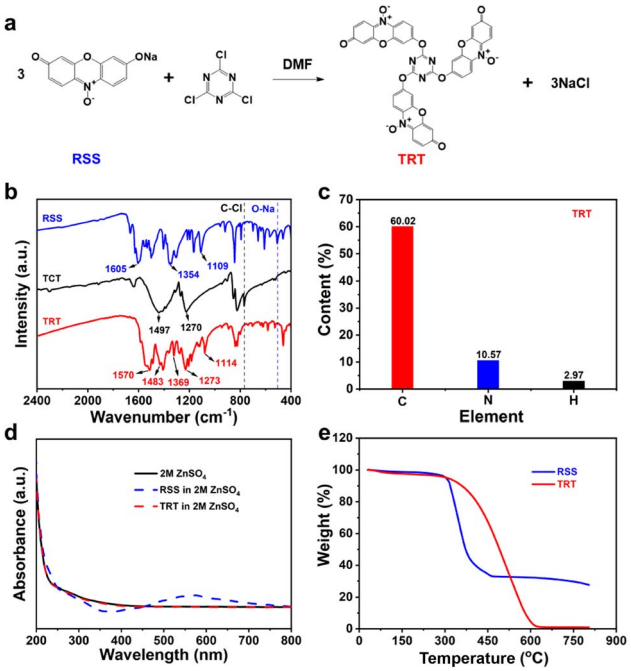

Fig. 1 (a) Synthesis procedure of TRT. (b) FT-IR spectra of RSS, TCT, and TRT. (c) Elemental analysis result of TRT. (d) The comparison of UV-vis spectra of RSS and TRT in the electrolyte (2 M $ZnSO_4$). (e) Thermogravimetric analysis of RSS and TRT.

(Fig. 1d) of TRT in electrolyte and bare electrolyte exhibit significant overlap. In contrast, the electrolyte containing RSS displays a distinct peak at 575 nm, proving that RSS is largely dissolved, while TRT remains insoluble. In addition, the thermal stability of RSS and TRT was investigated *via* thermogravimetric analysis (TGA). Fig. 1e demonstrates the decomposition behavior of both RSS and TRT. RSS started decomposing at around 300 °C, whereas TRT exhibited higher thermal stability, with decomposition occurring at approximately 350 °C, indicating superior thermal stability. Additionally, RSS was found to remain partially undecomposed even at a temperature of approximately 630 °C due to the presence of sodium. The sodium in RSS reacted with the surrounding air, forming sodium-containing compounds. In contrast, TRT underwent nearly complete thermal decomposition, indicating the absence of inactive sodium within its structure. This observation further supports the successful synthesis of TRT.

Detailed morphology and elemental composition information were acquired using scanning electron microscopy (SEM) and energy-dispersive X-ray spectroscopy (EDS). Fig. S1a† illustrates the cross-linked sheet structure of RSS, whereas the SEM image in Fig. S1b† depicts the porous and layered stacked three-dimensional architecture of TRT. These pores can act as pathways for Zn ions, enhancing the efficiency of electron and ion transportation. The energy-dispersive X-ray spectroscopy (EDS) mapping results in Fig. S2† demonstrate the uniform distribution of the key elements, such as carbon (pink), nitrogen (blue), and oxygen (red) within TRT. The nitrogen adsorption method was employed to examine the porous structure of TRT, and the absorption–desorption isotherms at 77 K are presented in Fig. S3.† These isotherms indicate an average pore size of 3.2 nm, classifying TRT as a mesoporous material. Furthermore, TRT exhibits a specific surface area of 4.0 $m^2\ g^{-1}$, which is advantageous for substantial zinc ion storage owing to its large aperture and high specific surface area.

Additionally, a two-probe technique was applied to measure the electronic conductivities of the pressed samples (RSS and TRT) at room temperature (Fig. S4†). The conductivity of TRT was measured to be 8.29×10^{-8} S m^{-1}, which is higher than that of RSS (2.53×10^{-9} S m^{-1}). The result demonstrates that the highly conjugated structure of TRT can facilitate the improvement of electronic conductivity.

Furthermore, density functional theory (DFT) calculations enabled a deeper comprehension of the molecular structure–property relationship concerning the organic cathode, as illustrated in Fig. 2a and b.[51] The calculated highest occupied molecular orbital–lowest unoccupied molecular orbital (HOMO–LUMO) gaps for the optimized molecule models are 0.678 eV (RSS, Fig. 2a) and 0.517 eV (TRT, Fig. 2b), respectively. The narrower energy gap of TRT contributes to its superior electronic conductivity for electrochemical zinc storage. Furthermore, the significantly increased density of states (DOS) of TRT crossing the Fermi level (Fig. S5†) will facilitate charge transfer, indicating an enhanced electronic conductivity.[52]

To assess the electrochemical performance, coin-type cells were constructed using the prepared electrode as the cathode, zinc foil as the anode, and a 2.0 M $ZnSO_4$ electrolyte. Fig. 2c and d depict the cyclic voltammetry (CV) curves of TRT and RSS, respectively. During the initial scan, a reduction peak was observed at 0.49 V, followed by an oxidation peak at 0.89 V. In the second cycle, two reduction peaks were detected, and subsequent scans revealed the merging of the two reduction

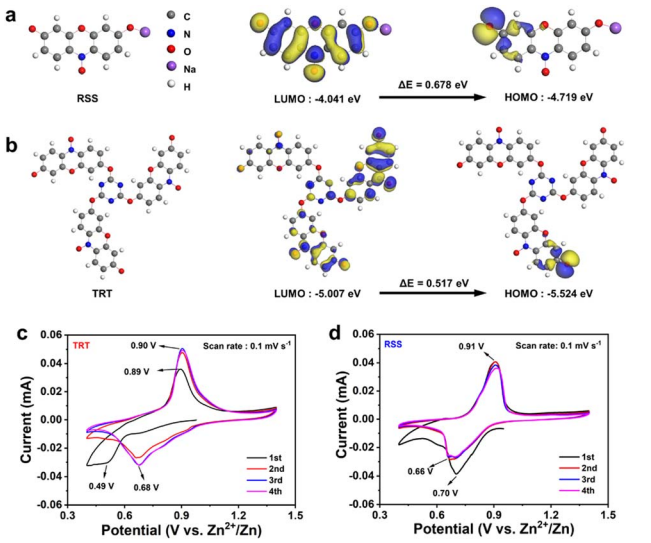

Fig. 2 Theoretical simulations of RSS and TRT. Calculated HOMO and LUMO of (a) RSS and (b) TRT. CV curves of (c) TRT and (d) RSS under 0.1 mV s^{-1}.

peaks at 0.68 V, while the oxidation peak shifted to 0.90 V. The variation in the redox peaks between the first two cycles and the subsequent cycles can be attributed to an activated process during battery operation. As the number of cycles increased, the redox peaks remained consistent, and the CV curves nearly overlapped, indicating excellent cycle stability and high reversibility. In the case of RSS, the CV profiles displayed a reduction peak at 0.70 V in the first cycle, while an oxidation peak was observed at 0.91 V. In subsequent sweeps, the reduction peaks split into two parts (at 0.66 V and 0.70 V), and the oxidation peaks did not exhibit significant shifts.

Fig. 3a illustrates the cycling ability of TRT at a current density of 100 mA g^{-1}, demonstrating that the specific discharge capacity remains at 110 mA h g^{-1} (with a coulombic efficiency of 99.5%) after 100 cycles. The similarity of the charge/discharge plateau between TRT and RSS in Fig. 3b suggests that the active sites of RSS were well-preserved. Besides, the charge/discharge plateau of TRT is observed at 0.90 V/0.68 V, respectively, which is consistent with the results of CV analysis. It can be observed that TRT maintains its original charge/discharge plateau even after undergoing 100 cycles, and the specific discharge capacity of TRT was demonstrated to be more than twice that of RSS after 100 cycles, indicating the highly conjugated structure of TRT not only inhibits the dissolution in the electrolyte but also improves the electrical conductivity. The TRT//Zn battery was subjected to various current densities ranging from 0.1 to 2.0 A g^{-1} for investigation. As illustrated in Fig. 3c, the discharge capacities were observed to be 170, 128, 105, 90, 83, and 78 mA h g^{-1} at current densities of 0.1, 0.2, 0.5, 1.0, 1.5, and 2.0 A g^{-1}. Meanwhile, Fig. 3d illustrates the charge/discharge curves of TRT and RSS at various current densities. Notably, the electrochemical plateau is almost absent in the high current density charge/discharge curve of RSS, while TRT exhibits obvious charge/discharge plateaus even at 2.0 A g^{-1}. The conjugated and porous structure of TRT facilitates electron and ion transport, which may account for its excellent rate performance. Furthermore, to assess the stability of TRT, long-term cyclability was investigated at a high current density of 500 mA g^{-1} (Fig. 3e). After 1000 cycles, TRT maintained a discharge capacity of approximately 65 mA h g^{-1} with an average coulombic efficiency of 99.8%, indicating exceptional cycling stability. Conversely, RSS only retained a discharge capacity of around 60 mA h g^{-1} after just 65 cycles. Although introducing a triazine ring structure will increase molecular weight (M_w), thus leading to a reduction of capacity, more importantly, the triazine ring has an abundance of nitrogen element and a highly conjugated structure. Introducing triazine rings in TRT can significantly increase electron delocalization, enhance the degree of conjugation and inhibit the dissolution in aqueous electrolyte, improving electrical conductivity and cycle performance.

To conduct a comprehensive investigation into the storage kinetics of Zn^{2+}, cyclic voltammetry (CV) curves were collected under varying scan rates ranging from 0.1 mV s^{-1} to 2.0 mV s^{-1}, as shown in Fig. 4a and c. The shapes of the redox peaks for both RSS and TRT remain consistent with increasing scan rates,

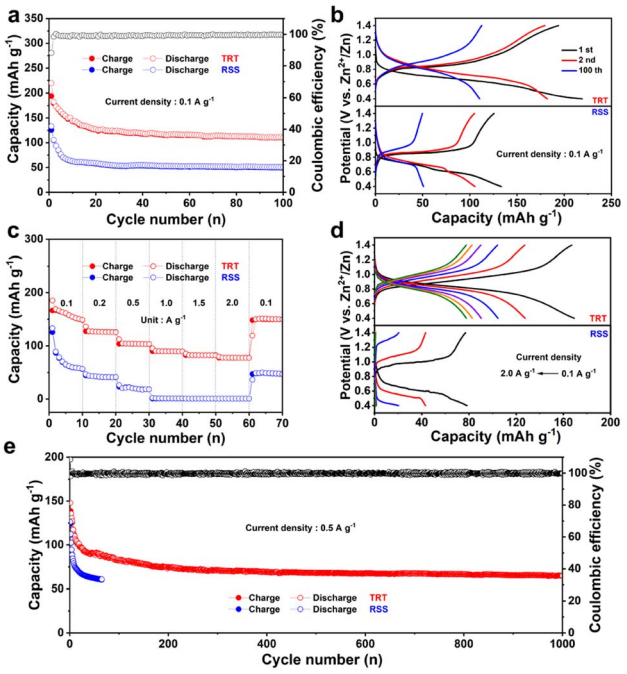

Fig. 3 Electrochemical tests. (a) Cycling performance of TRT and RSS at a current density of 0.1 A g^{-1}, and (b) corresponding charge/discharge profiles at different cycles. (c) Rate performances of TRT and RSS. (d) The comparison of charge/discharge profiles of TRT and RSS at different current densities from 0.1 to 2.0 A g^{-1}. (e) Long-term cyclability of TRT at a current density of 500 mA g^{-1} for 1000 cycles.

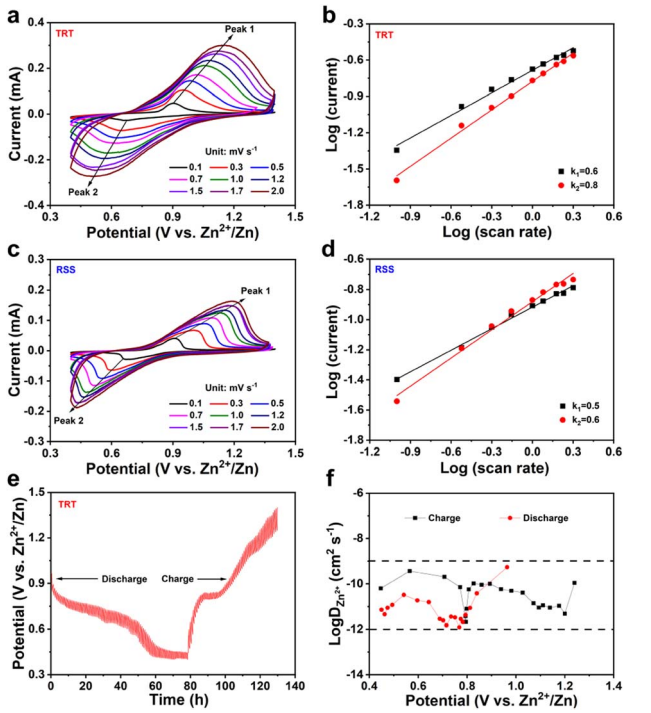

Fig. 4 (a and c) CV curves of TRT and RSS under different scan rates from 0.1 to 2.0 mV s^{-1}. (b and d) *b* values of TRT and RSS. (e) GITT curves of the TRT electrode and (f) corresponding Zn^{2+} diffusion coefficients.

indicating excellent cycle stability and high reversibility. However, as the scan rates increase, the reduction peak potential decreases while the oxidation peak shifts to a higher potential. The analysis between capacitive behavior and diffusion-controlled processes relies on the two following equations:

$$i = av^b \quad (1)$$

$$\log(i) = b\log(v) + \log(a) \quad (2)$$

Eqn (1) depicts the functional correlation between scan rate (v) and current (i), while the b value serves as a distinguishing factor for the capacity storage mechanism. Eqn (2) is derived from a logarithmic transformation of eqn (1). Upon examining eqn (2), it is evident that a linear correlation exists between log i and log v, where the slope represents the value of b. When b is close to 0.5, diffusion control governs the electrochemical behaviour. Conversely, when capacitive control dominates, b approaches a value of 1.[20] Fig. 4b and d depict the log i *vs.* log v plots, with TRT exhibiting the b values of 0.6 and 0.8, indicating a cathode dynamic that encompasses both capacitive behaviour and diffusion-controlled processes. In contrast, RSS displays the b values of 0.5 and 0.6, suggesting that diffusion control dominates its cathode dynamics.

Fig. S6a† presents the electrochemical impedance spectroscopy (EIS) measurements employed to examine the material's electrochemical performance.[53] The semicircle diameter in the Nyquist plots represents charge transfer resistance (R_{ct}).[54,55] We obtained Nyquist plots of TRT under different cycles (5th, 20th, and 50th). The three Nyquist plots exhibited a significant level of overlap, indicating that even after fifty cycles, the electrochemical performance of TRT remained as good as it was at the beginning, further underscoring its stable cycling behavior. Furthermore, Fig. S6b† demonstrates a decrease in R_{ct} from 1609 Ω during the fifth cycle to 1050 Ω after 50 cycles, indicating remarkable long-term cycling stability. The diffusion kinetics of Zn^{2+} were analyzed using galvanostatic intermittent titration technique (GITT) measurements (Fig. 4e), and the resulting data was combined with eqn (3) to determine the digitized value of Zn^{2+} diffusion coefficient ($D_{Zn^{2+}}$),

$$D_{Zn^{2+}} = \left(\frac{4L^2}{\pi\tau}\right) \times \left(\frac{\Delta E_s}{\Delta E_t}\right)^2 \quad (3)$$

where L stands for the diffusion length of Zn^{2+} (Fig. S7†) and τ corresponds to the relaxation time. The calculated zinc ion diffusion coefficients ($D_{Zn^{2+}}$) are shown in Fig. 4f, revealing that the diffusion coefficients of the zinc ion range from 1.24×10^{-12} to 5.38×10^{-10} cm^2 S^{-1} under different charge/discharge states. The $D_{Zn^{2+}}$ values are stable and high, which implies stable and rapid Zn^{2+} diffusion kinetics.

To further investigate the storage mechanism of TRT in AZIBs, *ex situ* FTIR and *ex situ* EPR were conducted to provide compelling evidence for this study. The active functional groups were analyzed by comparing the FTIR spectra at different charge and discharge potentials during the second cycle. Fig. 5a exhibits the second charge/discharge curves for a cell. The FTIR spectra obtained at various potentials are presented in Fig. 5b. The peak observed at 1570 cm^{-1} is attributed to carbonyl groups (C=O), while the peak observed at 1369 cm^{-1} corresponds to the nitroxide radical (N–O$^{\bullet}$). During the discharging process, the absorption intensity of N–O$^{\bullet}$ decreases with increasing discharging depth, whereas during charging, it gradually increases with increasing potential. This observation suggests that N–O$^{\bullet}$ undergoes a reversible redox reaction during the charging and discharging process. Similarly, the FTIR absorption peak intensity of C=O decreases during discharging and recovers during charging, indicating that both N–O$^{\bullet}$ and C=O are active functional groups in TRT and serve as active sites for Zn^{2+} binding. The absorption peak intensity of these groups is closely correlated with the degree of charging and discharging. Furthermore, the EPR results depicted in Fig. 5c demonstrate that the reversible peak intensity of the nitroxide radical exhibits a decrease and increase, respectively, during the charging and discharging processes, indicative of the reversibility of the N–O$^{\bullet}$.[56]

Theoretical calculations based on density functional theory (DFT) were carried out to further understand the storage mechanism of TRT. All constructed structures were optimized by the B3LYP method with the 6-31G(d, p) basis set for the TRT molecule, while for the adsorbed metal ion (Zn^{2+}), the lanl2dz basis set was employed. All calculations were performed using the Gaussian16 software package.[51] The TRT model, a centrosymmetric model with all atoms in the same plane, is constructed as shown in Fig. S8.† We analyzed the structural changes and relative electron energies of the carbonyl group (C=O), nitroxide radical (N–O$^{\bullet}$), and N atom in the triazine ring (N) after absorption of Zn^{2+} by theoretical calculation and showed them in Fig. S9.† Although the electronegativity of the N atom in the triazine ring is strong, the corresponding Zn^{2+} absorption (mode 3) exhibits the highest relative electron

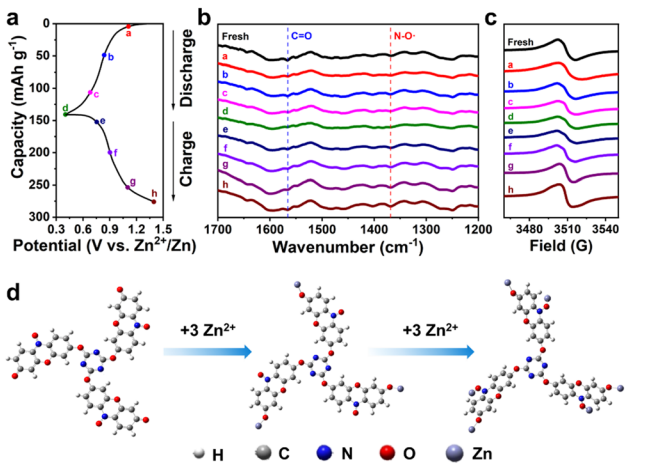

Fig. 5 *Ex situ* FTIR and EPR analysis of the TRT electrode. (a and b) FTIR spectra and (c) EPR signals under different discharge/charge states in the 2nd cycle: discharged from 1.4 to 0.4 V and then recharged to 1.4 V. (d) Theoretical calculation of the most stable Zn storage states: TRT, TRT-3Zn, and TRT-6Zn.

energy (ΔE) and terrible structural distortion compared to the other modes. By contrast, the C=O and N–O˙ sites (modes 1 and 2) display lower ΔE and stable structure. Therefore, based on the minimum energy principle, Zn ions preferentially react with the C=O and N–O˙ groups. According to the natural bond orbital (NBO) charge analysis calculation and lowest energy principle, both carbonyl and nitroxide radicals can be used as active sites in electrochemical redox reactions. Fig. 5d presents the binding of 6 Zn ions to TRT, where the active sites are the carbonyl groups and nitroxyl radicals. Fig. S10† displays three possible adsorption conformations, accompanied by their respective relative electron energies (in eV). It is evident that the carbonyl groups and nitroxyl radicals exhibit the lowest relative electron energy and minimal molecular structure changes when acting as zinc ion reaction sites. The theoretical results are consistent with the experimental results. TRT consists of double-active functional groups of carbonyl groups and nitroxyl radicals. It can react with 6 zinc ions, and the theoretical capacity is 211 mA h g^{-1}. However, the measured capacity is slightly lower than the theoretical value, possibly due to factors such as the burial of certain active functional groups.

Furthermore, to investigate the involvement of H^+ in the charging and discharging reactions, a three-electrode system test was conducted in this study. TRT served as the working electrode, Pt acted as the counter electrode, and Ag/AgCl (saturated with potassium chloride) was used as the reference electrode. CV tests were performed in 2 M $ZnSO_4$ and 1 M H_2SO_4 electrolytes, as shown in Fig. S11.†[57,58] As depicted in Fig. S11,† in the 2 M $ZnSO_4$ electrolyte, two reduction peaks were observed at −0.1 V and −0.05 V, accompanied by an oxidation peak at 0.28 V. In the 1 M H_2SO_4 electrolyte, redox peaks appeared at 0.36 V and 0.33 V. Notably, after shifting, it was revealed that the two CV curves exhibited some degree of overlap, providing the evidence that the cathode (TRT) can store not only Zn^{2+} but also H^+.

Conclusions

In conclusion, this study reported a method to improve the electrochemical performance of a small-molecule organic cathode material with active sites consisting of carbonyl and nitroxide radical functionalities. The preparation of conjugated TRT allows us to effectively address solubility and low conductivity concerns while preserving the electrochemical activity of RSS and eliminating non-redox active sites (Na). Consequently, it demonstrated improved electrical conductivity, superior specific capacity, extended cycle life, and enhanced rate performance compared to RSS. TRT offers a high reversible capacity of 180 mA h g^{-1} and maintains a capacity of 78 mA h g^{-1} even at a current density of 2 A g^{-1}. Also, it can cycle 1000 times at a current density of 0.5 A g^{-1}. This study offers a prospective organic cathode material for AZIBs, along with a promising desalination approach that mitigates the solubility issue of organic cathode materials in electrolytes and improves conductivity. These advancements enhance the reversible capacity, rate performance, and cycle stability of organic electrodes, thus showcasing the potential for improved AZIB performance.

Data availability

The data that support the findings of this study are openly available online.

Author contributions

H. B. L., W. B. and C. F. Z. designed and guided this experiment. W. W. and Y. T. carried out the experiment and materials characterization. J. L., R. W., L. H. Z., F. L. and L. Z. contributed to the data analysis and co-wrote the paper. H. B. L., W. B. and C. F. Z. proposed and supervised the project.

Conflicts of interest

There are no conflicts to declare.

Acknowledgements

We are thankful for the financial support from the National Natural Science Foundation of China (52172173, 51872071), Natural Science Foundation of Anhui Province for Distinguished Young Scholars (2108085J25), Excellent Research and Innovation Team Project of Anhui Province (2022AH010001), Natural Science Foundation of Anhui Province (2208085QE130), Distinguished Youths Research Project of Anhui Province (2022AH020013), and the Open Fund of Guangdong Provincial Key Laboratory of Advance Energy Storage Materials (AESM202106). We acknowledge the High-performance Computing Platform of Anhui University for providing computing resources.

Notes and references

1 S. Lee, G. Kwon, K. Ku, K. Yoon, S. K. Jung, H. D. Lim and K. Kang, *Adv. Mater.*, 2018, **30**, e1704682.
2 J. Y. Piao, L. Gu, Z. Wei, J. Ma, J. Wu, W. Yang, Y. Gong, Y. G. Sun, S. Y. Duan, X. S. Tao, D. S. Bin, A. M. Cao and L. J. Wan, *J. Am. Chem. Soc.*, 2019, **141**, 4900–4907.
3 Z. Wang, Y. Wang, C. Wu, W. K. Pang, J. Mao and Z. Guo, *Chem. Sci.*, 2021, **12**, 8945–8966.
4 R. Xu, G. Wang, T. Zhou, Q. Zhang, H.-P. Cong, S. Xin, J. Rao, C. Zhang, Y. Liu, Z. Guo and S.-H. Yu, *Nano Energy*, 2017, **39**, 253–261.
5 J. Zhou, S. Zhang, Y.-N. Zhou, W. Tang, J. Yang, C. Peng and Z. Guo, *Electrochem. Energy Rev.*, 2021, **4**, 219–248.
6 J. J. Shea and C. Luo, *ACS Appl. Mater. Interfaces*, 2020, **12**, 5361–5380.
7 Y. Lu, Q. Zhang, L. Li, Z. Niu and J. Chen, *Chem*, 2018, **4**, 2786–2813.
8 S. Zhang, L. Qiu, Y. Zheng, Q. Shi, T. Zhou, V. Sencadas, Y. Xu, S. Zhang, L. Zhang, C. Zhang, C.-L. Zhang, S.-H. Yu and Z. Guo, *Adv. Funct. Mater.*, 2021, **31**, 2006425.
9 R. M. Gao, H. Yang, C. Y. Wang, H. Ye, F. F. Cao and Z. P. Guo, *Angew. Chem., Int. Ed. Engl.*, 2021, **60**, 25508–25513.

10 K. Zhu, C. Guo, W. Gong, Q. Xiao, Y. Yao, K. Davey, Q. Wang, J. Mao, P. Xue and Z. Guo, *Energy Environ. Sci.*, 2023, DOI: 10.1039/D3EE01724A.
11 Y. Lyu, J. A. Yuwono, P. Wang, Y. Wang, F. Yang, S. Liu, S. Zhang, B. Wang, K. Davey, J. Mao and Z. Guo, *Angew. Chem., Int. Ed. Engl.*, 2023, **62**, e202303011.
12 N. Merukan Chola and R. K. Nagarale, *J. Electrochem. Soc.*, 2020, **167**, 100552.
13 Z. Wang, Y. Wang, B. Li, J. C. Bouwer, K. Davey, J. Lu and Z. Guo, *Angew. Chem., Int. Ed. Engl.*, 2022, **61**, e202206682.
14 T. Sun, Z. J. Li, Y. F. Zhi, Y. J. Huang, H. J. Fan and Q. Zhang, *Adv. Funct. Mater.*, 2021, **31**, 2010049.
15 K. W. Nam, H. Kim, Y. Beldjoudi, T. W. Kwon, D. J. Kim and J. F. Stoddart, *J. Am. Chem. Soc.*, 2020, **142**, 2541–2548.
16 N. Wang, X. Dong, B. Wang, Z. Guo, Z. Wang, R. Wang, X. Qiu and Y. Wang, *Angew. Chem., Int. Ed. Engl.*, 2020, **59**, 14577–14583.
17 R. Wang, S. Xin, D. Chao, Z. Liu, J. Wan, P. Xiong, Q. Luo, K. Hua, J. Hao and C. Zhang, *Adv. Funct. Mater.*, 2022, **32**, 2207751.
18 Z. Liu, R. Wang, Q. Ma, J. Wan, S. Zhang, L. Zhang, H. Li, Q. Luo, J. Wu, T. Zhou, J. Mao, L. Zhang, C. Zhang and Z. Guo, *Adv. Funct. Mater.*, 2023, DOI: 10.1002/adfm.202214538.
19 J. Wan, R. Wang, Z. Liu, L. Zhang, F. Liang, T. Zhou, S. Zhang, L. Zhang, Q. Lu, C. Zhang and Z. Guo, *ACS Nano*, 2023, **12**, 1610–1612.
20 Y. Tang, H. Kang, J. Zheng, H. Li, R. Wang, L. Zhang, Q. Ma, X. Xiong, T. Zhou and C. Zhang, *J. Power Sources*, 2022, **520**, 230895.
21 W. Wang, S. Wang, L. Zhang, S. Hu, X. Xiong, T. Zhou and C. Zhang, *Res. Appl. Mater. Sci.*, 2022, **4**, 31–41.
22 T. Kakeya, A. Nakata, H. Arai and Z. Ogumi, *J. Power Sources*, 2018, **407**, 180–184.
23 W. Wu, H.-Y. Shi, Z. Lin, X. Yang, C. Li, L. Lin, Y. Song, D. Guo, X.-X. Liu and X. Sun, *Chem. Eng. J.*, 2021, **419**, 129659.
24 S. Liu, J. P. Vongsvivut, Y. Wang, R. Zhang, F. Yang, S. Zhang, K. Davey, J. Mao and Z. Guo, *Angew. Chem., Int. Ed. Engl.*, 2023, **62**, e202215600.
25 W. Liu, J. Hao, C. Xu, J. Mou, L. Dong, F. Jiang, Z. Kang, J. Wu, B. Jiang and F. Kang, *Chem. Commun.*, 2017, **53**, 6872–6874.
26 H. Luo, B. Wang, J. Jian, F. Wu, L. Peng and D. Wang, *Mater. Today Energy*, 2021, **21**, 100799.
27 X. Guo, J. Zhou, C. Bai, X. Li, G. Fang and S. Liang, *Mater. Today Energy*, 2020, **16**, 100396.
28 P. Hu, T. Zhu, X. Wang, X. Zhou, X. Wei, X. Yao, W. Luo, C. Shi, K. A. Owusu, L. Zhou and L. Mai, *Nano Energy*, 2019, **58**, 492–498.
29 H. Yu, M. Aakyiir, S. Xu, J. D. Whittle, D. Losic and J. Ma, *Mater. Today Energy*, 2021, **21**, 100757.
30 Y. Liu, P. Hu, H. Liu, X. Wu and C. Zhi, *Mater. Today Energy*, 2020, **17**, 100431.
31 T. Xue and H. J. Fan, *J. Energy Chem.*, 2021, **54**, 194–201.
32 G. Li, L. Sun, S. Zhang, C. Zhang, H. Jin, K. Davey, G. Liang, S. Liu, J. Mao and Z. Guo, *Adv. Funct. Mater.*, 2023, DOI: 10.1002/adfm.202301291.
33 J. Wang, A. E. Lakraychi, X. Liu, L. Sieuw, C. Morari, P. Poizot and A. Vlad, *Nat. Mater.*, 2021, **20**, 665–673.
34 Z. Ye, S. Xie, Z. Cao, L. Wang, D. Xu, H. Zhang, J. Matz, P. Dong, H. Fang, J. Shen and M. Ye, *Energy Storage Mater.*, 2021, **37**, 378–386.
35 H. Glatz, E. Lizundia, F. Pacifico and D. Kundu, *ACS Appl. Energy Mater.*, 2019, **2**, 1288–1294.
36 H. Y. Shi, Y. J. Ye, K. Liu, Y. Song and X. Sun, *Angew. Chem., Int. Ed. Engl.*, 2018, **57**, 16359–16363.
37 P. Xiong, S. Zhang, R. Wang, L. Zhang, Q. Ma, X. Ren, Y. Gao, Z. Wang, Z. Guo and C. Zhang, *Energy Environ. Sci.*, 2023, DOI: 10.1039/d3ee01360j.
38 N. Kilic, S. Yesilot, S. Sariyer, A. Ghosh, A. Kilic, O. Sel and R. Demir-Cakan, *Mater. Today Energy*, 2023, **33**, 101280.
39 Y. Deng, C. Teng, Y. Wu, K. Zhang and L. Yan, *ChemSusChem*, 2022, **15**, e202102710.
40 Z. Guo, Y. Ma, X. Dong, J. Huang, Y. Wang and Y. Xia, *Angew. Chem., Int. Ed.*, 2018, **57**, 11737–11741.
41 C. Guo, Y. Liu, L. Wang, D. Kong and J. Wang, *ACS Sustainable Chem. Eng.*, 2021, **10**, 213–223.
42 Z. Tie and Z. Niu, *Angew. Chem., Int. Ed. Engl.*, 2020, **59**, 21293–21303.
43 X. Ma, X. Cao, M. Yao, L. Shan, X. Shi, G. Fang, A. Pan, B. Lu, J. Zhou and S. Liang, *Adv. Mater.*, 2022, **34**, e2105452.
44 Z. Wang, Q. Fan, W. Guo, C. Yang and Y. Fu, *Adv. Sci.*, 2022, **9**, e2103632.
45 J. Xie, P. Gu and Q. Zhang, *ACS Energy Lett.*, 2017, **2**, 1985–1996.
46 Q. Zhao, W. Huang, Z. Luo, L. Liu, Y. Lu, Y. Li, L. Li, J. Hu, H. Ma and J. Chen, *Sci. Adv.*, 2018, **4**, eaao1761.
47 O. Buyukcakir, J. Ryu, S. H. Joo, J. Kang, R. Yuksel, J. Lee, Y. Jiang, S. Choi, S. H. Lee, S. K. Kwak, S. Park and R. S. Ruoff, *Adv. Funct. Mater.*, 2020, **30**, 2003761.
48 Y. Zheng, S. Xia, F. Dong, H. Sun, Y. Pang, J. Yang, Y. Huang and S. Zheng, *Adv. Funct. Mater.*, 2021, **31**, 2006159.
49 W. Deng, W. Shi, Q. Liu, J. Jiang, Q. Wang and C. Guo, *J. Power Sources*, 2020, **479**, 228796.
50 S. Gu, S. Wu, L. Cao, M. Li, N. Qin, J. Zhu, Z. Wang, Y. Li, Z. Li, J. Chen and Z. Lu, *J. Am. Chem. Soc.*, 2019, **141**, 9623–9628.
51 M. J. Frisch, G. E. Scuseria, M. A. Robb, J. R. Cheeseman, G. Scalmani, V. Barone, B. Mennucci, G. A. Petersson, H. Nakatsuji, M. Caricato, X. Li, H. P. Hratchian, A. F. Izmaylov, J. Bloino, G. Zheng, J. L. Sonnenberg, M. Hada, M. Ehara, K. Toyota, R. Fukuda, J. Hasegawa, M. Ishida, T. Nakajima, Y. Honda, O. Kitao, H. Nakai, T. Vreven, J. A. Montgomery Jr, J. E. Peralta, F. Ogliaro, M. Bearpark, J. J. Heyd, E. Brothers, K. N. Kudin, V. N. Staroverov, R. Kobayashi, J. Normand, K. Raghavachari, A. Rendell, J. C. Burant, S. S. Iyengar, J. Tomasi, M. Cossi, N. Rega, J. M. Millam, M. Klene, J. E. Knox, J. B. Cross, V. Bakken, C. Adamo, J. Jaramillo, R. Gomperts, R. E. Stratmann, O. Yazyev, A. J. Austin, R. Cammi, C. Pomelli, J. W. Ochterski, R. L. Martin,

K. Morokuma, V. G. Zakrzewski, G. A. Voth, P. Salvador, J. J. Dannenberg, S. Dapprich, A. D. Daniels, O. Farkas, J. B. Foresman, J. V. Ortiz, J. Cioslowski and D. J. Fox, *Gaussian 16 revision A.03*, Gaussian, Inc., Wallingford CT, 2016.

52 L. Zhang, R. Wang, Z. Liu, J. Wan, S. Zhang, S. Wang, K. Hua, X. Liu, X. Zhou, X. Luo, X. Zhang, M. Cao, H. Kang, C. Zhang and Z. Guo, *Adv. Mater.*, 2023, **35**, 2210082.

53 Q. Guo, C. Zhang, C. Zhang, S. Xin, P. Zhang, Q. Shi, D. Zhang and Y. You, *J. Energy Chem.*, 2020, **41**, 185–193.

54 S. Li, J. Shang, M. Li, M. Xu, F. Zeng, H. Yin, Y. Tang, C. Han and H. M. Cheng, *Adv. Mater.*, 2022, e2207115.

55 C. Zhang, H. Li, X. Zeng, S. Xi, R. Wang, L. Zhang, G. Liang, K. Davey, Y. Liu, L. Zhang, S. Zhang and Z. Guo, *Adv. Energy Mater.*, 2022, **12**, 2202577.

56 Z. Wang, X. Zou, Y. Xie, H. Zhang, L. Hu, C. C. S. Chan, R. Zhang, J. Guo, R. T. K. Kwok, J. W. Y. Lam, I. D. Williams, Z. Zeng, K. S. Wong, C. D. Sherrill, R. Ye and B. Z. Tang, *Mater. Horiz.*, 2022, **9**, 2564–2571.

57 W. Wang, V. S. Kale, Z. Cao, S. Kandambeth, W. Zhang, J. Ming, P. T. Parvatkar, E. Abou-Hamad, O. Shekhah, L. Cavallo, M. Eddaoudi and H. N. Alshareef, *ACS Energy Lett.*, 2020, **5**, 2256–2264.

58 X. Wang, Y. Liu, Z. Wei, J. Hong, H. Liang, M. Song, Y. Zhou and X. Huang, *Adv. Mater.*, 2022, **34**, e2206812.